Electrochemical Deposition of Zn3P2 Thin Film Semiconductors Based on Potential–pH Diagram of the Zn-P-H2O System

AUTHOR(S):

Nose, Yoshitaro; Hosokawa, Kouhei; Uda, Tetsuya; Awakura, Yasuhiro

CITATION:

Nose, Yoshitaro ...[et al]. Electrochemical Deposition of Zn3P2 Thin Film Semiconductors Based on Potential–pH Diagram of the Zn-P-H2O System. Journal of The Electrochemical Society 2012, 159(4): D181-D186

ISSUE DATE:

2012-01

URL:

http://hdl.handle.net/2433/154847

Journal of The Electrochemical Society, **159** (4) D181-D186 (2012) D181
0013-4651/2012/159(4)/D181/6/$28.00 © The Electrochemical Society

Electrochemical Deposition of Zn_3P_2 Thin Film Semiconductors Based on Potential–pH Diagram of the Zn-P-H_2O System

Yoshitaro Nose,[z] Kouhei Hosokawa, Tetsuya Uda, and Yasuhiro Awakura

Department of Materials Science and Engineering, Kyoto University, Kyoto 606-8501, Japan

In this paper, we report on our attempt to make a thin film of Zn_3P_2 compound semiconductor by electrodeposition from aqueous solutions containing zinc and phosphorus species. First of all, we constructed the potential-pH diagram of the Zn-P-H_2O system at 363 K and found out the wide stable region of Zn_3P_2 at lower potentials. In the cyclic voltammetry on SnO_2 glass substrate, two cathodic current changes and an anodic peak were observed. This is similar results to Soliman et al., where the electrodeposition of Zn_3P_2 was succeeded. Consequently, the potentiostatic electrolysis thus was carried out to clarify the reduced substance and the reduction of SnO_2 was only observed. When Au electrode was used as an inert electrode, the formation of Zn_3P_2 was not also observed, while the Au-Zn compound was confirmed. It is considered that the precipitation of zinc predominantly occurs and the reduction of phosphate ions are kinetically difficult from the results of the cyclic voltammetry.
 [DOI: 10.1149/2.003204jes]

Manuscript submitted March 1, 2011; revised manuscript received September 30, 2011. Published January 18, 2012.

In recent years, solar cells are expected as an alternative energy since energy crisis is more serious. Substrates for solar cells have been mainly fabricated with Si crystals. However, it is important to reduce material consumption of pure Si for reductions in cost. Consequently, solar cells using compound semiconductors have been investigated because. Above all, solar cells using CdTe with II-IV type semiconductor and $CuInSe_2$ (CIS) or $Cu(In,Ga)Se_2$ (CIGS) with chalcopyrite-type structure have high efficiency approaching to Si solar cells[1] and these can be thin film because of their high coefficient for light absorption. However, there are some problems: the use of Cd which is toxic in CdTe solar cells and the use of In or Ga which are rare elements for CIS and CIGS. Therefore, the material without these elements is desired.

From the above background, we concentrated on Zn_3P_2 compound semiconductor as a solar absorber for solar cells. Zn_3P_2 has a direct bandgap of 1.5 eV,[2] which is suitable for energy conversion from sunlight to electricity, and a relatively high light absorption coefficient. Therefore, Zn_3P_2 is a promising candidate for the material of solar cells. Wyeth and Catalano[3] investigated the contact properties between Zn_3P_2 and various metals, and solar cells using metal/Zn_3P_2 schottky contact have been investigated by some researchers. Above all, the Mg/Zn_3P_2 solar cell shows the conversion efficiency of 6% under 1 AM.[4] Zn_3P_2 thin film has been mainly fabricated by gas phase growth, e.g. evaporation,[5–7] MOCVD[8,9] and RF-sputtering.[10] These methods are in vacuum at high temperatures, and take a high cost for apparatus. Recently, Soliman et al. have first reported an electrodeposition of Zn_3P_2 from aqueous solution containing zinc and phosphorus species.[11] The electrolysis using aqueous solution is a process at normal temperatures and pressures. Additionally, it is possible to electrodeposit thin films on the substrate with large area or complicated shapes. Therefore, the electrolysis is expected as a convenient and a low-cost process to obtain thin films for solar cells.

In this paper, we report on our attempt to make a thin film of Zn_3P_2 compound semiconductor by electrodeposition from aqueous solution. First of all, we construct the potential-pH diagram of the Zn-P-H_2O system and discuss on electrochemical behavior in the solution containing zinc and phosphorus species based on the diagram.

Potential–pH Diagram of the Zn–P–H_2O System

A potential–pH diagram is a powerful tool for understanding various electrochemical phenomena.[12] In this study, we construct the potential–pH diagram of Zn-P-H_2O system to understand electrodeposition behavior of Zn_3P_2 previous to experiments. In order to construct a potential–pH diagram of Zn-P-H_2O system, two diagrams of the Zn-H_2O and P-H_2O are necessary. They were derived according to the method by Pourbaix.[12] The thermodynamic data for the construction of potential-pH diagram are listed in Table I. Here, we defined the activity a_M of dissolved substance M with its molar concentration [M] in molarity (mol/dm^3), and the fugacity f_g of gaseous species g with its partial pressure p_g in atmosphere (atm). Since the electrolytic experiments were carried out at 363 K, the potential-pH diagram at the temperature was attempted. Unfortunately, some thermodynamic data at 363 K were not available, and we thus evaluated them by the following procedure.

For crystal species in Table I, we can obtain thermodynamic data at higher temperature from database.[13] The data for aqueous species were evaluated by the following equation,[14]

$$\Delta G_i^\circ[T] = \Delta G_i^\circ[298] - (T - 298)\,\Delta S_i^\circ[298], \qquad [1]$$

where $\Delta G_i^\circ[T]$ is the standard Gibbs energy for the formation of species i at temperature T and $\Delta S_i^\circ[298]$ is the standard entropy for the formation of species i at 298 K. The values calculated according to the above equation are also listed in Table I. Here, the standard entropy of $H_2PO_2^-$, $S^\circ_{H_2PO_2^-}[298]$, was estimated using the data of H_3PO_3 and $H_2PO_3^-$ since no data is available. The reaction for ionization of phosphorous acid, H_3PO_3, is expressed by

$$H_3PO_3 = H_2PO_3^- + H^+. \qquad [2]$$

The standard entropy change of the above reaction, $\Delta S^\circ(2)$, is evaluated by the following equation,

$$\Delta S^\circ(2) = S^\circ_{H_2PO_3^-} + S^\circ_{H^+} - S^\circ_{H_3PO_3}. \qquad [3]$$

The standard entropy change at 298 K was calculated to be –87.86 J/mol K using the thermodynamic data in Table I.

The ionization of hypophosphorous acid, H_3PO_2, and its entropy change are also expressed by

$$H_3PO_2 = H_2PO_2^- + H^+, \qquad [4]$$

and

$$\Delta S^\circ(4) = S^\circ_{H_2PO_2^-} + S^\circ_{H^+} - S^\circ_{H_3PO_2}. \qquad [5]$$

Both reactions of eqs. 2 and 4 are ionization reaction of hydrogen from OH belonging to tetrahedral $PO(OH)_2H$ or $PO(OH)H_2$ to produce proton (hydrogen ion) and also tetrahedral ions, $PO_2(OH)H$ or PO_2H_2.[15] Therefore, we expect the entropy change of eqs. 2 and 4 is similar. Actually, the standard entropy change of ionization of phosphoric acid, H_3PO_4, which is ionization of tetrahedral $PO(OH)_3$ to proton and $PO_2(OH)_2$, is –87.03 J/mol K that is similar to that of H_3PO_3. We thus assume that $\Delta S^\circ(4) = \Delta S^\circ(2)$, whereby we calculated the standard entropy of $H_2PO_2^-$ from eq. 5. Subsequently, we

[z] E-mail: yoshitaro-nose@mtl.kyoto-u.ac.jp

Table I. Thermodynamic data used in this study. The data marked by * were calculated and that by ** was estimated in this study. See the text for details.

Species	State	ΔG_i°[298] / kJ mol^{-1}	S_i°[298] / J mol^{-1} K^{-1}	ΔG_i°[363] / kJ mol^{-1}	Reference
Zn	Crystal	0	41.63	0	13
Zn^{2+}	Aqueous	−147.21	−106.48	−146.08*	16
Zn_3P_2	Crystal	−178.16	150.62	−174.21	13
ZnP_2	Crystal	−82.73	60.25	−78.37	13
P (red)	Crystal	−12.028	22.85	−10.7	13
P (white)	Crystal	0	41.07	0	13
H_3PO_4	Aqueous	−1147.25	176.15	−1116.62*	16
$H_2PO_4^-$	Aqueous	−1135.12	89.12	−1098.83*	16
H_3PO_3	Aqueous	−856.88	167.36	−832.35*	16
$H_2PO_3^-$	Aqueous	−846.63	79.5	−816.38*	16
H_3PO_2	Aqueous	−523.42	158.99	−505.01*	16
$H_2PO_2^-$	Aqueous	−512.12	71.13**	−488.00*	16
H^+	Aqueous	0	0	0	16
H_2O	Liquid	−236.96	69.87	−226.79	13
H_2	Gas	0	130.68	0	13
O_2	Gas	0	205.15	0	13
Sn	Crystal	0	51.195	0	13
SnO_2	Crystal	−520	53.342	−506.75	13

obtained the standard Gibbs energy for the formation of $H_2PO_2^-$ at 363 K according to eq. 1. It is noted that because the extrapolated temperature range in eq. 1 is only 65 K, we do not expect any serious error associated from above assumption.

Figure 1 shows the potential-pH diagrams in acid region for Zn-H_2O and P-H_2O systems. The activity of dissolving substance was set up to be 10^{-2} M. In this study, red phosphorus was regarded as a standard species of phosphorus, and phosphine, PH_3, was not considered. The diagrams were extended to the Zn-P-H_2O system. First, two diagrams of the Zn-H_2O and P-H_2O system were superimposed. The various formation reactions of Zn_3P_2 or ZnP_2 from zinc and phosphorus species were considered by the similar procedure as Murase et al.[16] For example, the boundary between $H_3PO_3 + Zn^{2+}$ and $H_3PO_3 + Zn_3P_2$ areas were determined by the reaction of the formation of H_3PO_3 and Zn_3P_2 from H_3PO_3 and Zn^{2+} shown by the following equation,

$$2H_3PO_3 + 3Zn^{2+} + 6H^+ + 8e = Zn_3P_2 + 6H_2O. \quad [6]$$

Figure 2 shows the potential-pH diagram of the Zn-P-H_2O system in acid region at 363 K under the activity of 10^{-2} M for dissolving substance and the partial pressure of 1 atm for H_2 and O_2 gases. From the figure, one can understand that there is the stable region of Zn_3P_2 shown by shadow that suggests the electrodeposition of Zn_3P_2 is possible by the reduction of aqueous species of zinc and phosphorus. However, in this case, the competition with the generation of H_2 gas due to its overpotential must be considered.

Experimental Procedure

Aqueous solution containing sodium metaphosphate, $NaPO_3$, and zinc dichloride, $ZnCl_2$, was used as an electrolyte for electrodeposition of Zn_3P_2 according to the experiments by Soliman et al.[11] $NaPO_3$ and $ZnCl_2$were dissolved in the deionized water with a specific resistance of larger than 5×10^6 Ωcm and their concentration is 10^{-2} M. The resistivity of the solution was 5×10^2 Ωcm. The dissolution of $NaPO_3$ produces H_3PO_4 and/or $H_2PO_4^-$ ion in acid region. The pH of the solution was measured by pH meter and adjusted to 2.5 using H_2SO_4 at room temperature, 298 K, whereas electrolytic experiments were carried out at 363 K. The three-electrode cell was used for all experiments. Figure 1 shows the schematic picture for the experimental system in this study. A SnO_2 conductive glass substrate (ASAHI GLASS Co. Ltd., resistivity: 10 Ωcm) or Au film

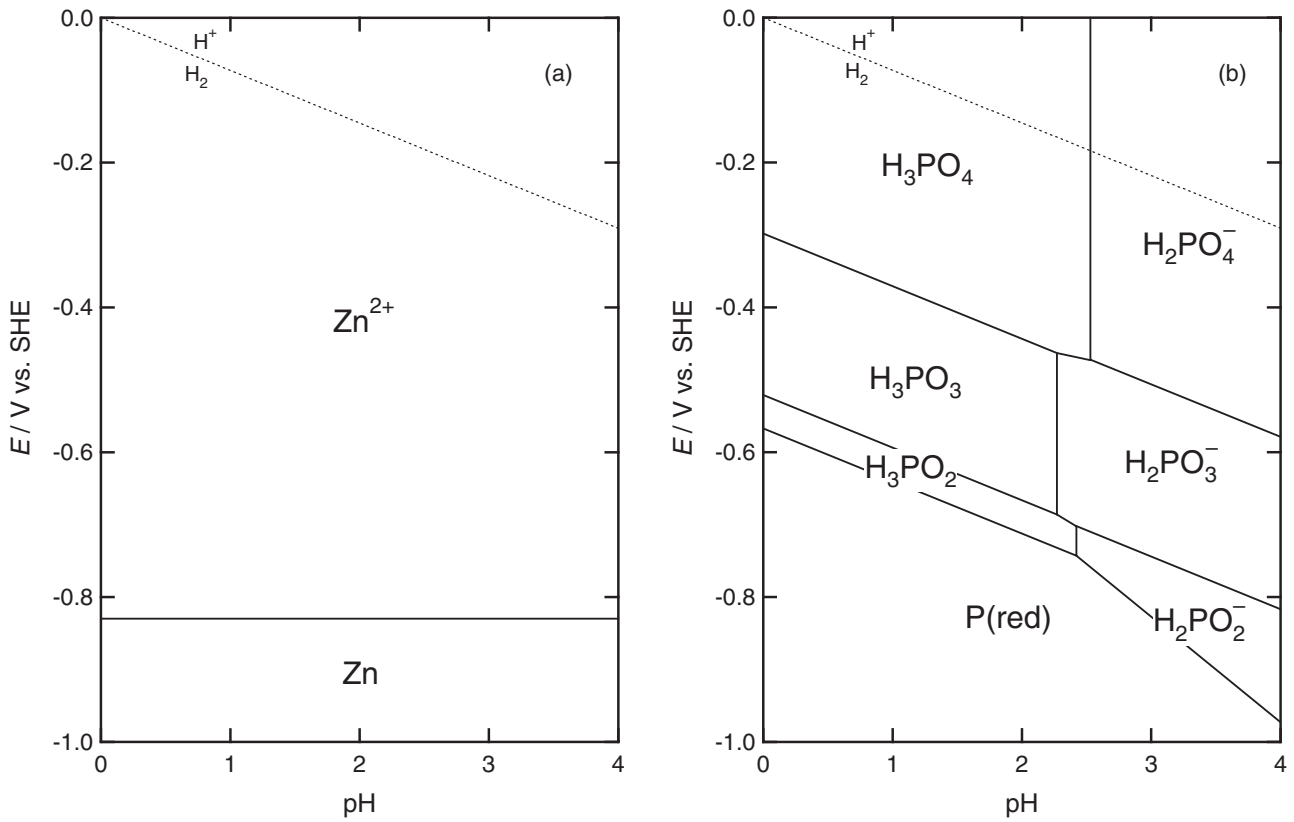

Figure 1. Potential-pH diagrams of (a) the Zn-H_2O and (b) the P-H_2O systems at 363 K, where the concentration of all aqueous species is 10^{-2} M.

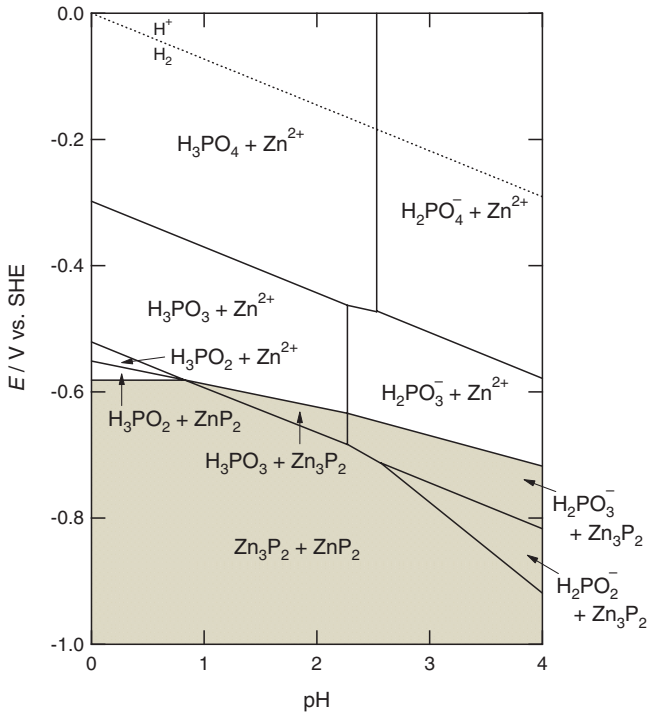

Figure 2. Potential-pH diagram of the Zn-P-H_2O system at 363 K, where the concentration of all aqueous species is 10^{-2} M. The shadow area shows the conditions to obtain Zn_3P_2.

electrodeposited on Cu plate were used as a working electrode, and a platinum sheet (20 mm × 30 mm) was used as a counter electrode (WE and CE in Fig. 3). Au film was electrodeposited by currentstatic electrolysis with the current density of 10 mA/cm^2 for 300 seconds using an aqueous solution containing $KAu(CN)_2$ of 14 g/dm^3, of $(NH_4)_2HPO_4$ of 70 g/dm^3 and K_2HPO_4 of 70 g/dm^3. The temperature of the solution was 343 K. The thickness of Au film was calculated to be about 3 μm from the current density. A part of the working electrode surface was covered with substrate holder made from polypropylene so that a known area (10 × 10 mm^2 or 15 × 15 mm^2) was exposed to the electrolyte as the surface of the working electrode. An Ag/AgCl electrode immersed in 3.3 M KCl was used as a reference electrode (RE). The electrode potentials were recalculated for standard hydrogen electrode (SHE). A glass vessel, which has the capacity of 250 cm^3, was used as an electrolyte cell. The volume of the electrolytic solution was 200 cm^3 and the temperature was controlled by the silicon rubber heater and the thermocouple. The actual temperature of the solution

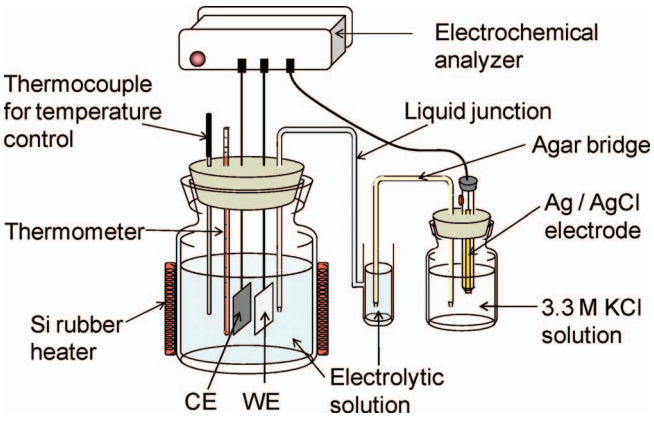

Figure 3. Schematic illustration of apparatus for electrochemical experiments.

was monitored by thermometer. Cyclic voltammetry and potentiostatic electrolysis were carried out using the electrochemical analyzer (ALS, 660A). In both experiments, the solution was not stirred. The product substance after electrolysis was identified by a grazing incident X-ray diffraction (GI-XRD, PANalytical X'Pert Pro) with a copper X-ray tube and the composition was evaluated by an energy dispersive X-ray spectroscopy (EDX, EDAX VE-9800) using a scanning electron microscope (SEM, KEYENCE VE-7800). The angle of the incident beam against the surface of the sample was 1° in GI-XRD.

Experimental Results and Discussion

Re-examination of electrodeposition on SnO_2.— Figure 4 shows the cyclic voltammogram on SnO_2 conductive glass for the solution containing $NaPO_3$ and $ZnCl_2$ together with the potential-pH diagram. The potential was swept from 0 V vs. SHE to a cathodic direction and subsequently switched at –0.59 V vs. SHE. We can observe two cathodic and an anodic current changes in the figure. The current change from –0.25 vs. SHE shown by 'a' in Fig. 4 is due to the reduction of proton to hydrogen gas considering from the potential-pH diagram. Another cathodic reaction was observed from –0.46 V vs. SHE that is shown by 'b'. This cathodic current change is caused from the reaction from $H_2PO_4^-$ to $H_2PO_3^-$, which is the reaction from a pentavalent to a tetravalent species, considering from the potential-pH diagram. The anodic current peak shown by 'c' was observed around at –0.23 V vs. SHE. This peak is considered to be a counter to the cathodic current change shown by 'b' because both current changes

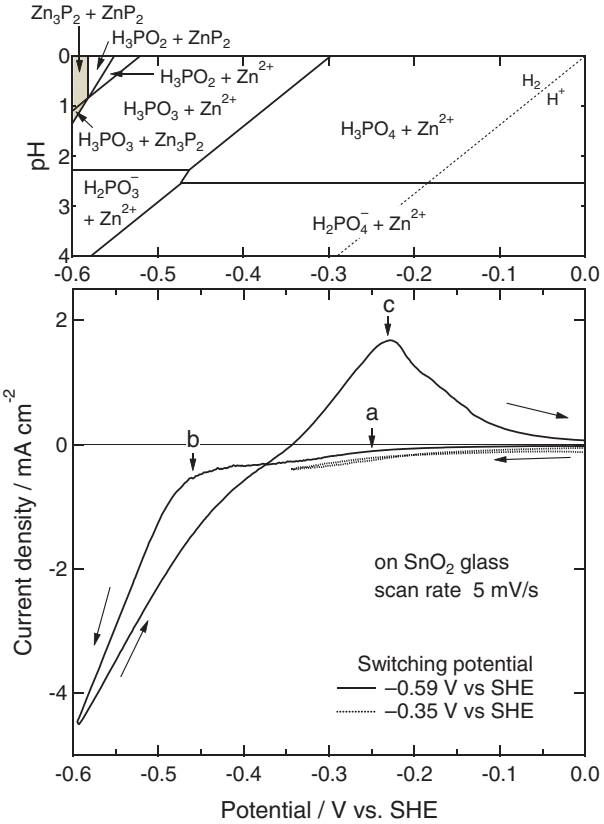

Figure 4. Cyclic voltammogram using the solution containing both $ZnCl_2$ and $NaPO_3$ and a part of potential-pH diagram of the Zn-P-H_2O system shown in Fig. 2. Solid and dotted lines in the cyclic voltammogram are the cases where the potential was switched at –0.59 V vs SHE and –0.35 V vs SHE, respectively. The arrows show the scan directions. The cathodic and the anodic currents are shown by negative and positive values, respectively.

did not appear when the potential was reversed at switching potential of –0.35 V vs. SHE as shown in Fig. 4.

Soliman et al. also observed two cathodic current changes at –0.62 V vs. SCE and –0.75 V vs. SCE, and an anodic current peak at –0.45 V vs. SCE in the cyclicvoltammetry. They used the saturated calomel electrode (SCE) as a reference. The equilibrium potential of the standard calomel electrode is about +0.24 V vs. SHE at 298 K and then we recalculated the potential for the standard hydrogen electrode in their study when we assume that the potential of the saturated calomel electrode does not change so much at 363 K; the above potentials were calculated to be –0.38 V vs. SHE, –0.51 V vs. SHE and –0.21 V vs. SHE, respectively.

Soliman et al. mentioned that the cathodic reaction at –0.38 V vs. SHE came from the reduction of expressed by the following equation,

$$4PO_3^- + 5e = P + 3PO_4^-. \quad [7]$$

However, the reduction from PO_3^- to metallic phosphorus is considered to be difficult because the stability region of metallic phosphorus is at lower potential than –0.38 V vs. SHE from the potential-pH diagram. In addition, PO_3^- is not stable in acid region. It is considered that this cathodic current change in their paper corresponds to the reduction of proton to hydrogen gas at –0.25 vs. SHE in this study. The second cathodic current change at –0.51 V vs. SHE was assigned to the reduction of zinc and accordingly the electrodeposition of Zn_3P_2 in the paper by Soliman et al. However, the reduction of zinc might be impossible since the equilibrium potential between Zn and Zn^{2+} is –0.83 V vs. SHE. The anodic current peak observed at –0.21 V vs. SHE is a counter to the cathodic current change at –0.51 V vs. SHE. Such a pair of current change was also observed in this study as mentioned above.

The results of the cyclicvoltammetry of this study are similar to that by Soliman et al., but the interpretation is different. Consequently, the potentiostatic electrolysis was carried out at –0.59 V vs. SHE for 1 hour in order to identify the reduced substance. The reduced substance was thus identified by GI-XRD and the results were shown in Fig. 5. The diffraction pattern of metallic tin was observed together with that of SnO_2 in the X-ray diffraction profile after electrolysis. On the other hand, the peaks from Zn_3P_2 were not observed although Soliman et al. confirmed the electrodeposition of Zn_3P_2. Here, the equilibrium potential between Sn and SnO_2 is –0.32 V vs. SHE at 363 K in the case of pH = 2.5, that was calculated using the data listed in Table I. Therefore, it is likely that the reduction of

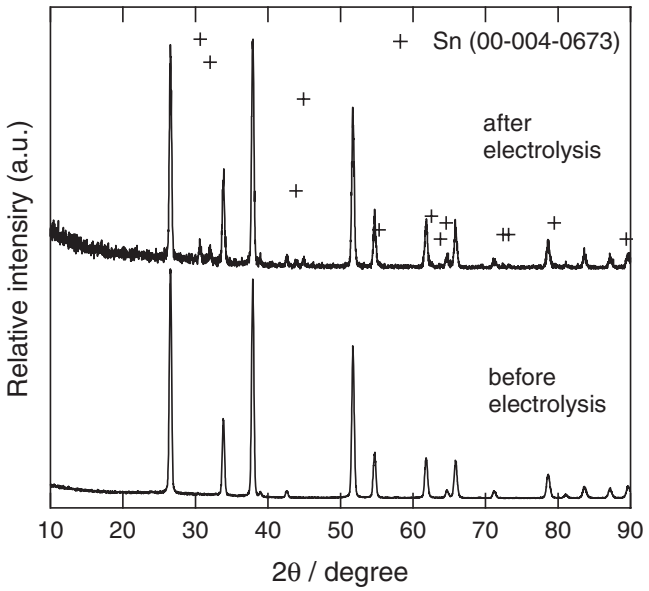

Figure 5. GI-XRD profiles of the SnO_2 glass substrate before and after the potentiostatic electrolysis.

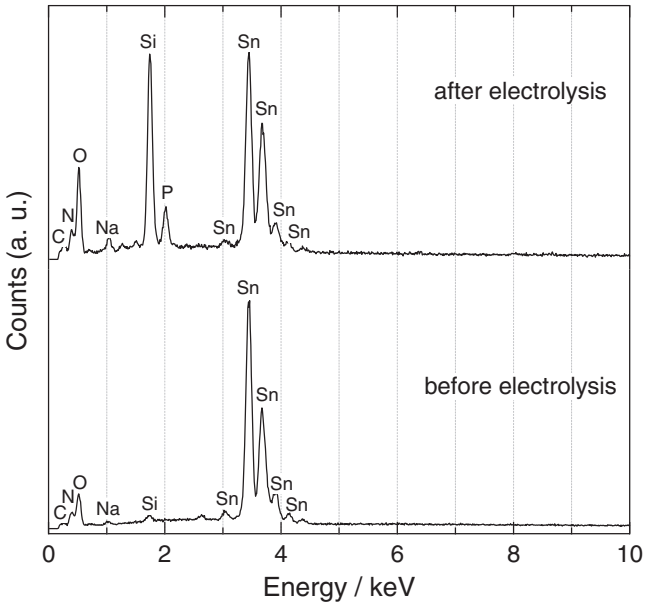

Figure 6. EDX profiles of the SnO_2 glass substrate before and after the potentiostatic electrolysis.

SnO_2 to metallic tin occurs in the potentiostatic electrolysis and the cyclicvoltammetry. Soliman et al. indentified the reduced substance as Zn_3P_2 by XRD. The peak positions of three strong lines for Zn_3P_2 and tin are listed in Table II. These positions are relatively near and it is considered that Soliman et al. might confuse the reduction of SnO_2 with the electrodeposition of Zn_3P_2. Figure 6 shows the EDX spectra before and after the electrolysis. Phosphorus was detected by EDX in the experiments where the reduction of SnO_2 was observed as shown in Fig. 6. It is considered that this comes from the adhesion of the electrolytic solution since the redox potential to obtain red phosphorus is lower than –0.59 V vs. SHE. On the other hand, the peaks of ZnLα and ZnKα, which should appear around at 1 keV and 8.6 keV, respectively, were not detected. Consequently, it is concluded that the formation of Zn_3P_2 did not occur in this condition.

Electrochemical behavior on Au electrode.— When using SnO_2 glass as WE, the formation of Zn_3P_2 was not observed due to the reduction of SnO_2. Consequently, Au film electrodeposited on Cu plate was used as an inert electrode. Figure 7 shows the cyclic voltammogram on Au electrode containing $NaPO_3$ and $ZnCl_2$. The cathodic current change was observed around at –0.25 V vs. SHE shown by 'a,' which was considered to come from the generation of hydrogen gas. In actual, the bubble was observed on the electrode during the measurements. Considering from the potential-pH diagram, the reduction of phosphoric acid would occur at –0.45 V vs. SHE, however, the notable current change was not observed in this study. Therefore, it is concluded that the cathodic current change observed in SnO_2 glass comes from the reduction of SnO_2 as previously mentioned.

Table II. Peak positions in XRD for Zn_3P_2 and Sn.

Substance (JCPDS card number)	Peak position (2θ/degree)	Relative intensity	Index
Zn_3P_2 (00-053-0591)	31.370	43	(004)
	32.235	47	(203)
	44.766	100	(224)
Sn (00-004-0673)	30.644	100	(200)
	32.018	90	(101)
	44.902	74	(220)

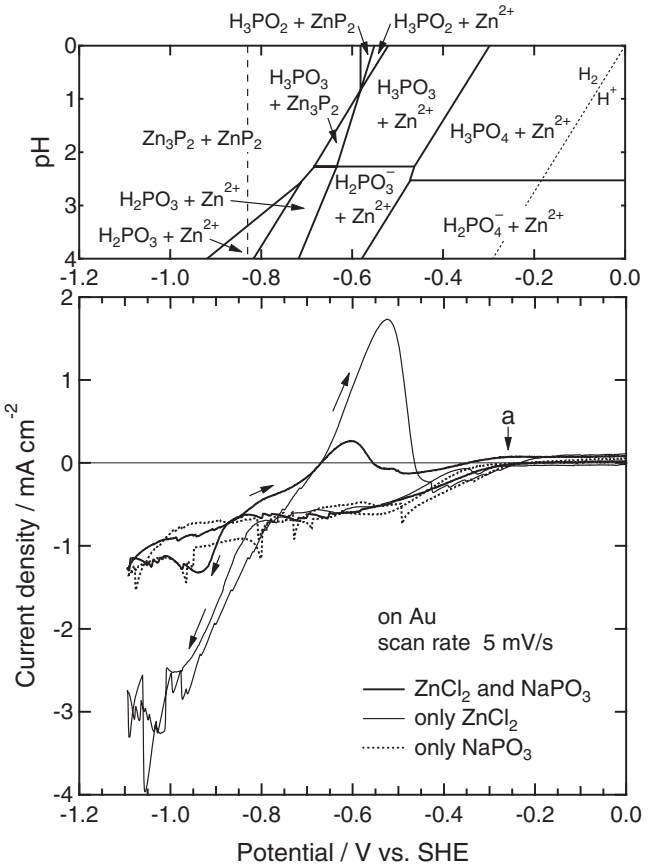

Figure 7. Cyclic voltammogram on Au electrode using each solution and a part of potential-pH diagram of the Zn-P-H_2O system shown in Fig. 2. The switching potential is –1.09 V vs SHE. The dashed line shows the equilibrium potential between Zn^{2+} and Zn in the potential-pH diagram.

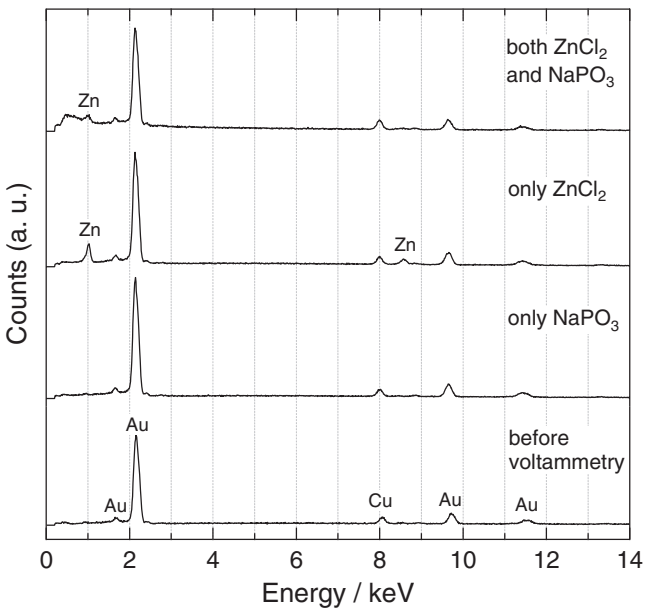

Figure 8. EDX profiles before and after the voltammetry when using Au electrode.

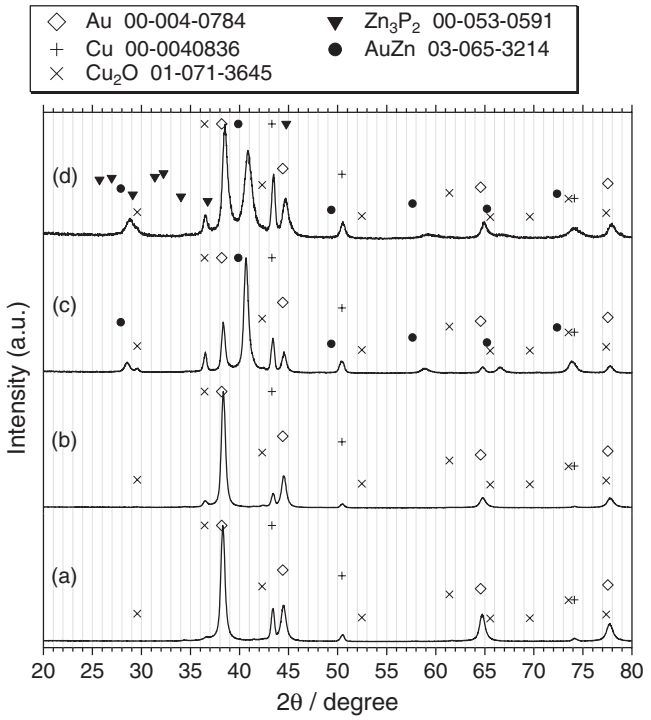

Figure 9. GI-XRD profiles of Au electrode (a) before the voltammetry, (b) $NaPO_3$ solution, (c) $ZnCl_2$ solution and (d) solution containing both $ZnCl_2$ and $NaPO_3$ after the voltammetry. Symbols show the reference data.

In order to investigate the electrodeposition of Zn_3P_2, the cyclic-voltammetry was carried out to the lower potentials. In this experiment, three kinds of electrolytic solution were prepared; $ZnCl_2$, $NaPO_3$, and both $ZnCl_2$ and $NaPO_3$. The concentration of each species was 0.01 M. Figure 7 shows the cyclic voltammogram where the switching potential is –1.09 V vs SHE, together with a part of potential-pH diagram of the Zn-P-H_2O system. The current change from –0.25 vs. SHE, which is observed in all solutions, is due to the reduction of proton to hydrogen gas. In the solution containing only $NaPO_3$, another current change is not observed and the upset of the current might come from the generation and the desorption of hydrogen gas on Au electrode. On the other hand, the cathodic current change was also observed at –0.8 V vs. SHE in the solution containing only $ZnCl_2$. The dashed line shows the equilibrium potential between Zn and Zn^{2+} in Fig. 7 and the current change is thus considered to be due to the reduction of Zn^{2+} to Zn. The cathodic current change was also observed at the lower potential in the solution containing both $ZnCl_2$ and $NaPO_3$. The origin of the current change is considered to be the reduction of Zn^{2+} or the formation of Zn_3P_2 considering from the potential-pH diagram and the results of other solutions. Figure 8 shows the results of EDX analysis before and after the cyclic voltammetry. The peaks related to Zn were observed in the solution containing both $ZnCl_2$ and $NaPO_3$ in addition to Au and Cu, while phosphorus was not detected. Figure 9 shows the results of GI-XRD after the cyclic voltammetry for each solution. The peaks of Au, Cu and Cu_2O were confirmed in the XRD profile before the experiments. A similar pattern was obtained in the solution containing only $NaPO_3$ after the cyclic voltammetry. On the other hand, additional peaks were found in the solutions containing $ZnCl_2$ as shown (c) and (d) in the figure. These peaks do not suggest the formation of Zn_3P_2 because they are observed even in the solution containing only $ZnCl_2$. The formation of AuZn is thus considered from the XRD profile. The additional peaks are observed at higher angle positions compared to reference data of AuZn. The formation of solid solution was reported for AuZn phase[17] and the difference of peak positions can be

understood by considering the deviation from the stoichiometry. The results of XRD are consistent with those by EDX.

The formation of Zn_3P_2 was not observed on Au electrode although it was suggested in the potential-pH diagram of the Zn-P-H_2O system. The reduction of Zn^{2+} was found in the solutions containing $ZnCl_2$, while that of phosphate ions was not observed in the solution containing only $NaPO_3$. It is assumed that the reduction of phosphate ions is kinetically difficult and the current was consumed for the reduction of zinc ions although the reduction of both ions are needed for the formation of Zn_3P_2. Therefore, the suppression of zinc precipitation might be necessary to obtain Zn_3P_2. One of considerations is the use of ligand for Zn^{2+}, which reduces the activity of Zn^{2+}.

Conclusions

In this paper, we investigated the electrodeposition of Zn_3P_2 semiconductor from aqueous solution. First, we constructed the potential-pH diagram of the Zn-P-H_2O system at 363 K and clarified the wide stable region of Zn_3P_2 at lower potentials. Subsequently, the cyclicvoltammetry was carried out in the same conditions as Soliman et al. and two cathodic current changes and an anodic peak were observed in the cyclicvoltamogram, where the potential was switched at –0.59 V vs. SHE. It was considered that these current changes were not related to the electrodeposition of Zn_3P_2 from the viewpoint of potential-pH diagram although Soliman et al. claimed the electrodeposition of Zn_3P_2. In the electrolysis experiment at –0.59 V vs. SHE for 1 hour, the reduction of SnO_2, which was used as a substrate, was observed. When Au electrode was used as an inert electrode, the formation of Zn_3P_2 was not also observed although it was suggested by the potential-pH diagram. One of reasons is that the reduction of phosphate ions are kinetically difficult. In order to obtain Zn_3P_2 by electrodeposition from aqueous solutions, it is necessary that the reduction of Zn^{2+} is suppressed and that of phosphate ions is enhanced.

Acknowledgments

This work was partly supported by the Ministry of Education, Culture, Sports, Science and Technology, Japan.

References

1. M. A. Green, K. Emery, Y. Hishikawa, W. Warta, and D. Dunlop, *Prog. Photovolt.*, **19**, 565 (2007).
2. E. A. Fagen, *J. Appl. Phys.*, **50**, 6505 (1979).
3. N. C. Wyeth and A. Catalano, *J. Appl. Phys.*, **51**, 2286 (1980).
4. M. Bhushan and A. Catalano, *Appl. Phys. Lett.*, **38**, 39 (1981).
5. A. Lousa, E. Bertran, M. Varela, and J. L. Morenza, *Sol. Energy Mater.*, **12**, 51 (1985).
6. K. R. Murali, *Mater. Sci. Eng.*, **92**, 193 (1987).
7. T. Suda, T. Nishimoto, and S. Kurita, *J. Cryst. Growth* **86**, 430 (1988).
8. J. Long, *J. Electrochem. Soc.*, **130**, 725 (1983).
9. A. M. Hermann, A. Madan, M. W. Wanlass, V. Badri, R. Ahrenkiel, S. Morrison, and C. Gonzalez, *Sol. Energy Mater. Sol. Cells*, **82**, 241 (2004).
10. T. Suda, T. Miyakawa, and S. Kurita, *J. Cryst. Growth*, **86**, 423 (1988).
11. M. Soliman, A. B. Kashyout, M. Osman, and M. El-Gamal, *Renewable Energy*, **30**, 1819 (2005).
12. M. Pourbaix, *Atlas of Electrochemical Equilibria in Aqueous Solutions*, Pergamon Press, Oxford, 1966.
13. I. Barin, *Thermodynamic data of pure substances*, 3rd ed., Wiley-VCH, Weinheim, 1995.
14. W. M. Latimer, *Oxidation Potentials*, 2nd ed., Prentice-Hall, New York, 1952.
15. P. W. Atkins, *Physical Chemistry*, 4th ed., Oxford University Press, Oxford, 1990.
16. K. Murase, H. Watanabe, T. Hirato, and Y. Awakura, *J. Electrochem. Soc.*, **146**, 1798 (1999).
17. T. B. Massalski, H. Okamoto, P. R. Subramanian, and L. Kacprzak, *Binary alloy phase diagram*, 2nd ed., ASM International, Materials Park, Ohio (1990).